Chapter 2
5-Axis Flank Milling of Sculptured Surfaces

Johanna Senatore, Frédéric Moniès and Walter Rubio

This chapter covers the various free-form surface flank milling strategies available, focusing in particular on those for ruled surfaces as widely used in defining turbomachine parts. All these positionings seek to reduce interference between the cutting tool and the surface to be milled so as to respect the tolerances dictated by the Design Office. The range of strategies presented goes from the simplest, using analytical positioning on a particular rule, through to complex procedures defined using global numerical methods that calculate the toolpath in its entirety. Approaches adapted to conical and half-barrel cutter geometries are also addressed. Machining of free-form surfaces is considered from two differing perspectives: either considering a free-form surface to be a set of ruled surfaces onto which the previously mentioned methods are applied, or studying the differential geometry of the cutters and surfaces.

2.1 Introduction

Flank milling involves machining a workpiece with the side part of the cutter. The cutter generatrices are generally straight lines (with a cylindrical or conical cutter) or arcs of circles (barrel cutter) (Fig. 2.1), but in some cases they can take other shapes.

This process is widely used in the industry for all contouring operations. The workpiece parts thus produced take the shape of planes, portions of cylinders or cones and more generally any type of developable surface. The advantage with

J. Senatore · F. Moniès · W. Rubio (✉)
Institut Clément Ader, Université Paul Sabatier,
118 route de Narbonne, Cedex 09, 31062, Toulouse, France
e-mail: rubio@cict.fr

J. P. Davim (ed.), *Machining of Complex Sculptured Surfaces*,
DOI: 10.1007/978-1-4471-2356-9_2,

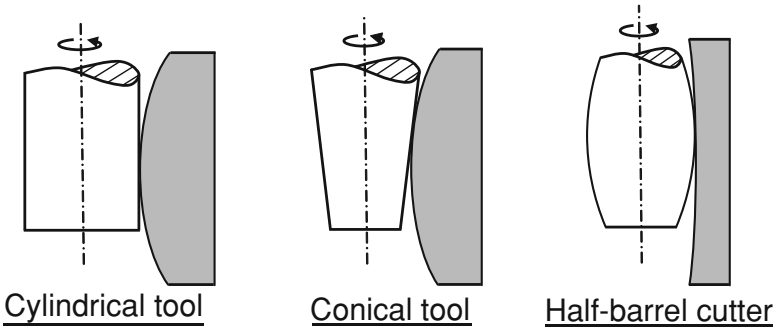

Fig. 2.1 Cutter geometries

Fig. 2.2 Impeller-type part

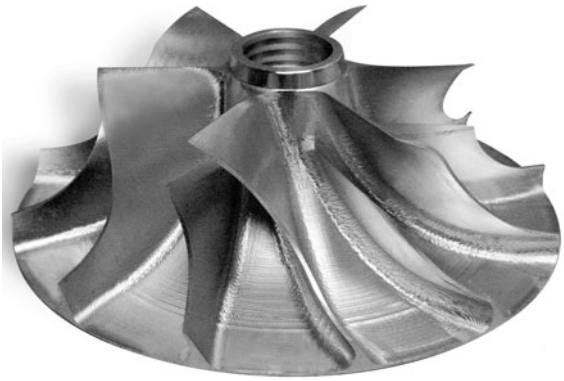

flank milling lies in removing a considerable amount of material and also permitting access to zones that would be inaccessible to end milling.

This milling method applies to other types of surfaces and is especially suited to convex free-form surfaces or surfaces with negative Gaussian curvatures that have one of their principal curvatures small compared with the cutter radius, being subject to only very slight change over the entire surface. Ruled surfaces answer to the previously stated criteria and are generally machined in this way. Such surfaces are mainly encountered on workpieces going into the manufacturing of turbomachines. Given their critical role and the stresses to which they are subjected, such high value added workpieces require special care. It is hardly surprising that such a substantial corpus of scientific works has been devoted to how they are machined with the aim of boosting productivity while respecting the quality levels required by the relevant specifications. Among such workpieces, the following are to be found:

- Impellers (Fig. 2.2): rotating parts used to suck in a liquid, or to diffuse or compress a gas. Impellers are provided with arrays of principal and secondary blades. The concave side and the convex side of these blades are generally modelled by non-developable ruled surfaces with reduced twist on the leading

Fig. 2.3 Inducer type part

and trailing edges and pronounced twist located towards the middle of the blade. Blade heights remain fairly low.

- Inducers (Fig. 2.3): rotating parts placed at the entry of an impeller with the aim of enhancing performance. They work to provide an overpressure so that the fluid does not cavitate into the main pump. The concave and convex sides are modelled by non-developable ruled surfaces whose twist is fairly high and regular.
- Fans (Fig. 2.4): rotating parts used to accelerate a fluid. They have a large number of short, high blades. The concave and convex sides are modelled by non-ruled free-form surfaces.

Flank milling's main advantage lies in increasing the width of the area machined as the cutter passes through. This leads to shorter machining times, lower production costs and greater productivity. Another positive outcome in increasing the cutting width lies in reducing polishing operations. Where surfaces can be milled in a single pass, no scallop of material is left behind the cutter and polishing operations are therefore much reduced. Before introducing machining strategies, a definition will be provided for ruled surfaces.

2.2 Ruled Surfaces

2.2.1 Definition

A surface containing a family of straight lines is called a ruled surface. It is generated by the movement of a straight line, called the rule or generatrix, moving over two curves $\mathbf{C_0}(\mathrm{u})$ and $C_1(\mathrm{u})$ that provide its directrices.

Ruled surfaces are often used to draw functional surfaces in mechanical engineering. They resolve the following problem: given two curves in space $\mathbf{C_0}(\mathrm{u})$ and $\mathbf{C_1}(\mathrm{u})$, both defined on the same parametric interval $\mathrm{u} \in [0, 1]$, find a surface $\mathbf{S}$ such that $\mathbf{S}(\mathrm{u}, 0) = \mathbf{C_0}(\mathrm{u})$ and $\mathbf{S}(\mathrm{u}, 1) = \mathbf{C_1}(\mathrm{u})$. The problem posed has an infinite number of solutions. Here, the following model will be retained:

Fig. 2.4 Fan type part

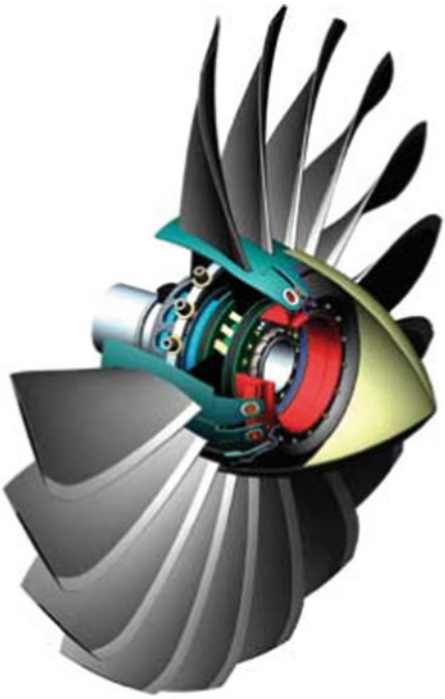

Fig. 2.5 Ruled surface

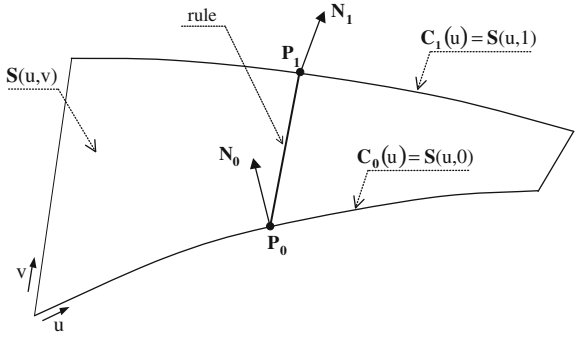

$$\mathbf{S}(u, v) = (1 - v)\ \mathbf{C_0}(u) + v\ \mathbf{C_1}(u) \quad (u, v) \in [0, 1]^2 \tag{2.1}$$

Ruled surfaces have the following property: each isoparametric line (parameter u constant), is called a rule, and is a straight line segment (Fig. 2.5). One major feature of such surfaces is the authorised generality for curves $\mathbf{S}(u, 0)$ and $\mathbf{S}(u, 1)$ that have practically no restriction other than being defined on the same parameter interval. For example, one of the entry curves can be a cubic polynomial curve, while the other can be a Bezier or a B-spline curve.

This surface definition is widely used when modelling workpieces for the aeronautical, naval and car industry sectors.

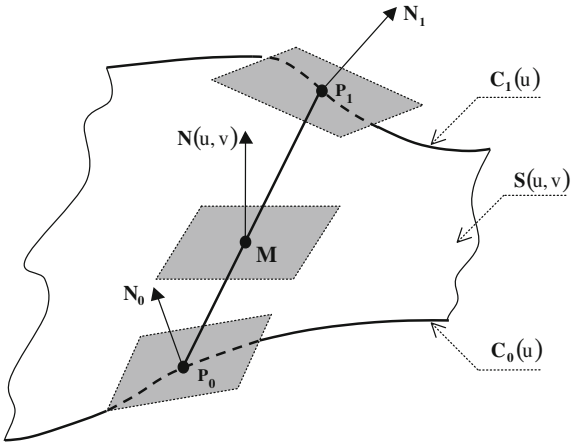

Fig. 2.6 Evolution of tangent planes on the rule $[\mathbf{P_0P_1}]$

The following notations will be used in the rest of this chapter:

- $\mathbf{S}(u, v)$ the surface to be machined,
- $\mathbf{N}(u, v)$ the normal to the surface $\mathbf{S}(u, v)$,
- $[\mathbf{P_0P_1}]$: the rule considered,
- $\mathbf{C_0}(u), \mathbf{C_1}(u)$: the directrices of the surface $\mathbf{S}(u, v)$,
- $\mathbf{N_0}$,$\mathbf{N_1}$: normal to $\mathbf{S}(u, v)$ on $\mathbf{P_0}$ and $\mathbf{P_1}$ respectively,
- α: the twist corresponding to the angle between normals $\mathbf{N_0}$ and $\mathbf{N_1}$:
- $\mathbf{h_p}$: the length of the rule $(\mathbf{P_0P_1})$.

Two types of ruled surfaces can be distinguished:

- Developable ruled surfaces: a surface is developable if its Gaussian curvature K is null and its mean curvature H non-null at any point. Calling $\mathbf{S_{uv}}(u, v)$ the second derivative of $\mathbf{S}(u, v)$ in relation to parameters u and v, this can be expressed by the statement: "$\mathbf{S}(u, v)$ is a developable ruled surface if and only if $\mathbf{N}(u, v) \cdot \mathbf{S_{uv}}(u, v) = 0$ at any point". It can be seen that the twist of a developable surface is null whatever the rule $[\mathbf{P_0P_1}]$ on the surface: $\alpha = 0$.
- Non-developable ruled surfaces: these can be characterised by one of the two following properties:

"Non-developable ruled surfaces have a non-null twist: $\alpha \neq 0$",

"Not all points located on a given rule have the same tangent plane" (Fig. 2.6).

To provide the background to the reasoning adopted in the present section, it will be useful first to conduct a preliminary analysis of the twist of non-developable ruled surfaces.

Evolution of the normals to $\mathbf{S}(u, v)$ along the rule will depend on curves $\mathbf{C_0}(u)$ and $\mathbf{C_1}(u)$. The normal to a surface is calculated by the vectorial product of the first derivatives. For the ruled surface the following will obtain:

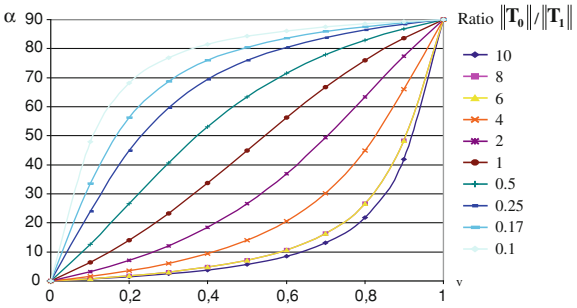

Fig. 2.7 Evolution of twist as a function of the ratio $\|\mathbf{T_0}\|/\|\mathbf{T_1}\|$

$$\mathbf{N}(u,v) = \frac{\partial \mathbf{S}(u,v)}{\partial u} \wedge \frac{\partial \mathbf{S}(u,v)}{\partial v} = \left((1-v)\frac{\mathbf{dC_0}(u)}{du} + v\frac{\mathbf{dC_1}(u)}{du}\right) \wedge \mathbf{P_0P_1} \quad (2.2)$$

Evolution of $\mathbf{N}(u,v)$ along the rule ($v \in [\mathbf{0},\mathbf{1}]$) will depend on $\frac{\mathbf{dC_0}(u)}{du}$ and $\frac{\mathbf{dC_1}(u)}{du}$. To simplify matters, it is assumed that $\frac{\mathbf{dC_0}(u)}{du}$ and $\frac{\mathbf{dC_1}(u)}{du}$, noted respectively $\mathbf{T_0}$ and $\mathbf{T_1}$, are perpendicular to $\mathbf{P_0P_1}$.

Let $\mathbf{T}_i = ((1-v)\mathbf{T_0} + v\mathbf{T_1})$, the evolution of $\mathbf{N}(u,v)$ will follow the evolution of $\mathbf{T_i}$. Let α_i be the angle between $\mathbf{T_0}$ and $\mathbf{T_i}$ as calculated by:

$$\cos(\alpha_i) = \frac{\mathbf{T_0} \cdot \mathbf{T}_i}{\|\mathbf{T_0}\|\|\mathbf{T}_i\|} = \frac{(1-v)\|\mathbf{T_0}\| + v\|\mathbf{T_1}\|\cos(\alpha)}{\|(1-v)\mathbf{T_0} + v\mathbf{T_1}\|} \quad (2.3)$$

The following is obtained:

$$\cos(\alpha_i) = \frac{(1-v)\frac{\|\mathbf{T_0}\|}{\|\mathbf{T_1}\|} + v\cos(\alpha)}{\sqrt{(1-v)^2\left(\frac{\|\mathbf{T_0}\|}{\|\mathbf{T_1}\|}\right)^2 + 2v(1-v)\left(\frac{\|\mathbf{T_0}\|}{\|\mathbf{T_1}\|}\right)\cos(\alpha) + v^2}} \quad (2.4)$$

This result is interesting as it shows that the evolution of the normal depends on the ratio between the norms of vectors $\mathbf{T_0}$ and $\mathbf{T_1}$. The evolution of α_i was plotted as a function of v (Fig. 2.7) for several values of the ratio $\|\mathbf{T_0}\|/\|\mathbf{T_1}\|$. With no loss in generality, in this example angle α of the twist equals 90°.

It can be seen that the evolution of the normal along the rule is not linear. However, linearity when the ratio between $\|\mathbf{T_0}\|$ and $\|\mathbf{T_1}\|$ is close to 1 can be considered. Such curves will be analysed later when focusing on strip milling.

2.2.2 Machining Non-Developable Ruled Surfaces

During flank milling of a non-developable ruled surface, the existence of twist α implies that it is impossible to machine the workpiece perfectly using a non-null diameter cutter, with the cutter positioning on the surface leading to inevitable

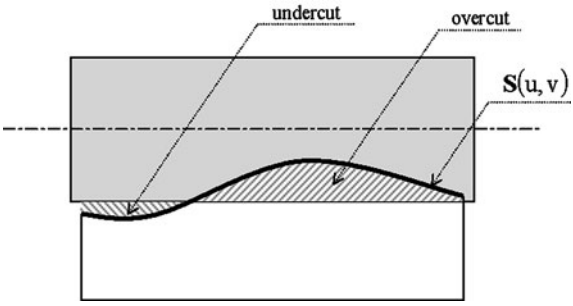

Fig. 2.8 Overcut and undercut errors

interference. It then becomes interesting to seek the positioning leading to minimal interference. This means that cutters with larger cross-sections can be used; these have good rigidity and ensure maximum material removal while respecting tolerance of the surface shape. This problem of cutter positioning optimisation involves the uses of 5-axis NC machine tools so as to be able to orient the cutter freely.

The interference error caused by the cutter during milling can be of two types: geometrical error corresponding to the maximum interference generated by the cutter for a given positioning, and machining error related to the cutting process environment and expressing the real behaviour of the cutter/workpiece/machine assembly (cutter bending, vibrations, etc.). The remainder of this section will focus on studying geometrical error.

The interference generated by the cutter is of two types (Fig. 2.8): either the cutter removes too much material (overcut), or the cutter leaves too much material behind it (undercut).

To calculate interference error, the distance between a point of the theoretical surface along its normal and the cutter is considered. This corresponds to the definition of the profile tolerance of any surface. To conclude on respect for tolerance of the machined surface, maximum undercut and overcut errors need to be compared with the imposed shape tolerance.

2.2.3 Local Positioning

When discussing tool positioning, this obviously does not concern developable ruled surfaces. Indeed, for such surfaces, the cutter causes no error due to positioning and problems of visibility (access to the surface) alone are to be considered. Few methods have been developed for cutter positioning during flank milling of non-developable ruled surfaces. Two main approaches can be distinguished:

- Analytical methods: this involves positioning methods that are generally simple to implement but that generate relatively significant errors. Chronologically speaking, these were the first methods to be published.

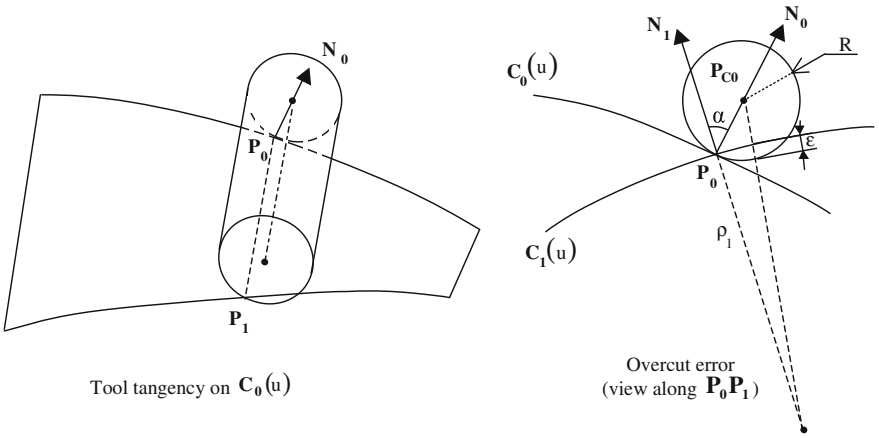

Fig. 2.9 Software positioning

- Numerical methods: these considerably reduce geometrical machining error but are more complex to implement. Their development was reliant on the enhancement of computing capacity.

2.2.3.1 Analytical Positioning

One of the first forms of analytical positioning to be implemented was of the kind to be found in many CAD/CAM software packages (referred to hereafter as "software positioning"). It was developed for cylindrical cutting tools and involves positioning the cutter axis parallel to the rule considered and the cutter tangent to a directrix (Fig. 2.9). Any interference between the cutter and the workpiece will then be concentrated on the other directrix. The cutter is tangent to directrix $\mathbf{C_0}(u)$, the cutter axis is collinear to vector $\mathbf{P_0P_1}$, and the maximum overcut error will be on $\mathbf{C_1}(u)$. Knowing the orientation of the cutter axis, determining positioning involves calculating a point of the axis $\mathbf{P_{C0}} = \mathbf{P_0} + \mathrm{R}\,\mathbf{N_0}$ (R cutter radius).

Maximum interference error ε is given by:

$$\varepsilon = \rho_1 + \mathrm{R} - \sqrt{\mathrm{R}^2 + \rho_1^2 + 2\rho_1 \mathrm{R}\cos\alpha} \tag{2.5}$$

with ρ_1 the radius of curvature on $\mathbf{P}_1$ of the directrix $\mathbf{C}_1(u)$. ρ_1 is assumed to be constant in the zone studied.

If the curvature ρ_1 is great compared with R then the error becomes:

$$\varepsilon = \mathrm{R}(1 - \cos(\alpha)) \tag{2.6}$$

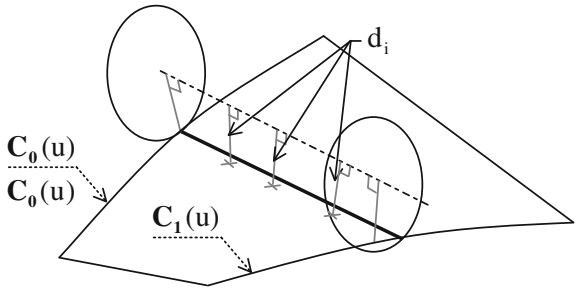

Fig. 2.10 CATS method, computing distances

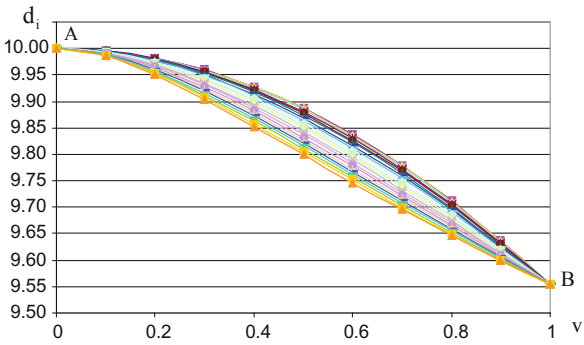

Fig. 2.11 Profile of the set of distances

The method developed in [1, 2] called Computation of Adapted Tool Shape (CATS) involves using software positioning and adapting it to the geometry of the cutter at the detected interferences. Thus, from evolution in the twist, the minimum distance d_i from the axis to the surface of the workpiece (Fig. 2.10) can be computed at each cross-section of the cutter, taken perpendicular to the axis. The distance from the cutter axis to $\mathbf{C_0}(u)$ is chosen equal to R (10 mm in the following example).

For all rules, distances d_i can be carried over onto a graph (Fig. 2.11). In the example below, all rules are considered to have the same length (30 mm). The cutter geometry is to be chosen from amongst all the curves and will depend on a number of criteria (minimising maximum error, preventing overcut and minimising the volume between the machined surface and the nominal surface). These criteria represent varying difficulties in implementation.

The selected cutter will have barrel geometry (Fig. 2.1) in order to simplify manufacturing. The cutter profile will be defined by a circle with radius Rt going through A and B (Fig. 2.11) and verifying a criterion. This method's advantage lies in the use of elementary positioning while minimising error by its compensation on the cutter diameter; it is especially appropriate to surfaces with a twist that varies little over the set of rules. This applies pretty well to inducers.

Rubio [3] also developed analytical positioning (referred to as standard positioning). The concept developed here involves the distribution of errors on each of the directrices of the surface. The axis of the cylindrical cutter is collinear to the

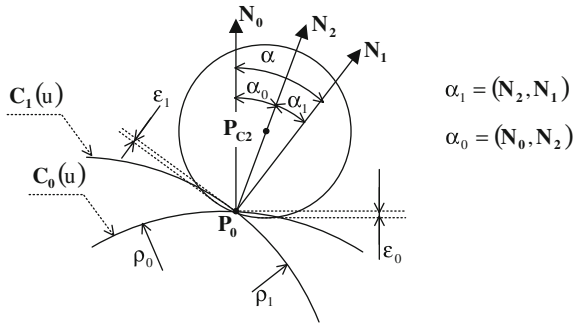

Fig. 2.12 Standard positioning (view along $\mathbf{P_0P_1}$)

rule considered and its position is defined by a point $\mathbf{P_{C2}}$ calculated such that interferences ε_0 and ε_1 on the directrices are equal.

The radii of curvatures ρ_0 and ρ_1 of the directrices $\mathbf{C_0}(u)$ and $\mathbf{C}_1(u)$ on P_0 and P_1 respectively are assumed to be constant locally. The maximum interference error ε_i $(i = 0, 1)$ located on the directrix $\mathbf{C_i}(u)$ can be expressed:

$$\varepsilon_\mathbf{i} = \rho_\mathbf{i} + R - \sqrt{R^2 + \rho_\mathbf{i}^2 + 2\rho_\mathbf{i} R \cos \alpha_\mathbf{i}} \tag{2.7}$$

The following system results from distribution of the error:

$$\begin{cases} \rho_0 + R - \sqrt{R^2 + \rho_0^2 + 2\rho_0 R \cos \alpha_0} = \rho_1 + R - \sqrt{R^2 + \rho_1^2 + 2\rho_1 R \cos \alpha_1} \\ \alpha = \alpha_0 + \alpha_1 \end{cases} \tag{2.8}$$

Angles $\alpha_\mathbf{0}$ and $\alpha_\mathbf{1}$ verifying $\varepsilon_\mathbf{0} = \varepsilon_1$, and vector $\mathbf{N}_2$ defined from the normals $\mathbf{N_0}$ and $\mathbf{N}_1$ (Fig. 2.12) defining the point $\mathbf{P_{C2}} = \mathbf{P_0} + R\mathbf{N}_2(u)$ can then be determined.

For surfaces showing large radii of curvature as compared with the cutter radius, $\alpha_0 = \alpha_1 = \alpha/2$ is obtained.

The resulting error is then equal to $\varepsilon = R(1 - \cos(\alpha/2))$. Through a series development of the cosine function, the error is estimated at $\varepsilon \approx R\alpha^2/8$ representing an error four times smaller than that for software positioning.

In the previous positioning methods, the cutter axis is collinear to the rule considered. Liu [4] proposes a new positioning adopting a different philosophy: here, the cutter swivels in relation to the rule. This positioning is known as "Double Point Offsets" (DPO).

Two corresponding points for the cutter axes, noted $\mathbf{C_A}$ and $\mathbf{C_B}$ (Fig. 2.13) are calculated from two points located at a quarter and three-quarters of the length of the rule, noted respectively **A** and **B**. These points $\mathbf{C_A}$ and $\mathbf{C_B}$ are determined by the following relations:

$$\mathbf{C_A} = \mathbf{A} + R\mathbf{N_A} \tag{2.9}$$

$$\mathbf{C_B} = \mathbf{B} + R\mathbf{N_B} \tag{2.10}$$

with: $\mathbf{N_A}$ and $\mathbf{N_B}$ the unit normals to the surface at points **A** and **B** respectively.

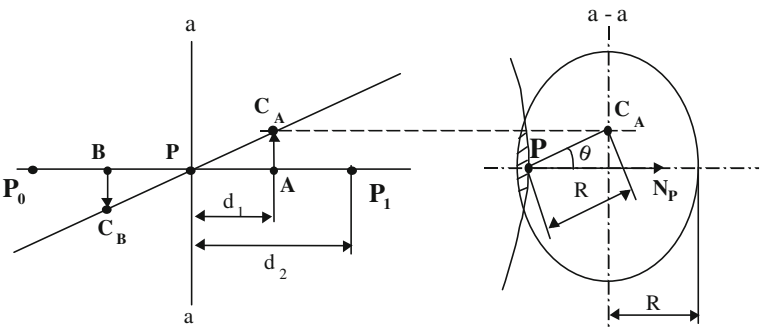

Fig. 2.13 Positioning Liu

The middle point of the rule is called **P** and the unit normal to the surface at that point is $\mathbf{N_P}$. Maximum interference induced by this positioning is of the undercut type ($\varepsilon_{PO,\,P1}$) at ends $\mathbf{P_0}$ and $\mathbf{P}_1$ of the rule and of the overcut type (ε_P) on **P**. These errors are calculated from the relations given below:

$$\varepsilon_P = R(1 - \cos\theta) \tag{2.11}$$

$$\varepsilon_{P0,P1} = R\left(\sqrt{\cos^2\theta + \frac{d_2^2}{d_1^2}\sin^2\theta} - \sqrt{1 + \frac{R^2 d_2^2 \sin^2\theta \tan^2\theta}{d_1^2\left(d_2^2\tan^2\theta + d_1^2 + R^2\sin^2\theta\right)}}\right) \tag{2.12}$$

The total error generated by this positioning is equal to the sum of these errors:

$$\varepsilon = \varepsilon_P + \varepsilon_{P0,P1} \tag{2.13}$$

The author then proposes to move the cutter along the normal $\mathbf{N_P}$ by a distance δ as determined algebraically, in order to distribute the error equally on either side of the theoretical surface. This distance can be determined algebraically by:

$$\delta = -\frac{\varepsilon_P + \varepsilon_{P0,P1}}{1 + \sqrt{\frac{d_1^2}{d_1^2 + d_2^2\tan(\theta)}}} \tag{2.14}$$

A first analytical positioning was described initially in [5]. This showed strong similarities with "DPO" positioning. The difference resides in the fact that the points of the cutter axis $\mathbf{P_{C0}}$ and $\mathbf{P_{C1}}$ are calculated from the end points of the rule:

$$\mathbf{P_{C0}} = \mathbf{P_0} + R\mathbf{N_0} \tag{2.15}$$

$$\mathbf{P_{C1}} = \mathbf{P_1} + R\mathbf{N_1} \tag{2.16}$$

The error is of the overcut type between the two ends of the rule. The maximum error is in the middle of the rule and the lowest overcut errors are located on $\mathbf{P_0}$ and $\mathbf{P}_1$. The cutter is then translated to distribute the interference error.

Figure 2.14 shows these different positioning methods.

Fig. 2.14 Software, standard and Liu positioning

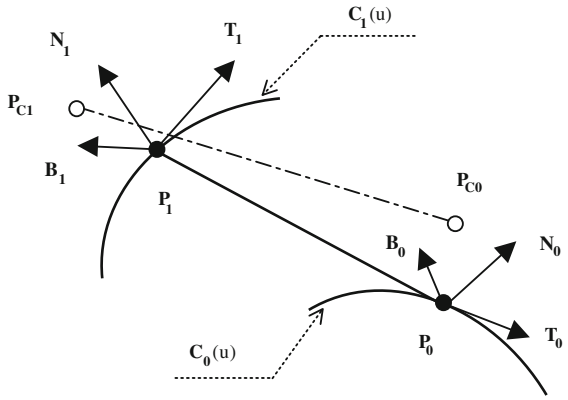

Fig. 2.15 Positioning Bedi

2.2.3.2 Numerical Positioning

Two types of numerical resolutions to position the cutter can be distinguished:

- methods relying on resolution of a system of *n* equations with *n* unknowns,
- iterative methods.

The presentation will now consider positioning obtained by system resolution.

In works by Bedi et al. [6], the cutter is positioned tangent to the two directrices at the ends of the rule (Fig. 2.15). The Frenet frames of curves $\mathbf{C_0}(u)$ and $\mathbf{C_1}(u)$ are placed at points $\mathbf{P_0}$ and $\mathbf{P_1}$. Vectors ($\mathbf{T_i}, \mathbf{N_i}$ and $\mathbf{B_i}$) represent vectors, tangents, normals and binormals. Positioning of the cutter axis is conducted from points $\mathbf{P_{C0}}$ and $\mathbf{P_{C1}}$. that verify the following conditions:

– $\mathbf{P_{C0}}$ et $\mathbf{P_{C1}}$ belong respectively to the planes $(\mathbf{P_0}, \mathbf{N_0}, \mathbf{B_0})$ and $(\mathbf{P_1}, \mathbf{N_1}, \mathbf{B_1})$
– $\|\mathbf{P_{C0}P_0}\| = \mathrm{R}$ and $\|\mathbf{P_{C1}P_1}\| = \mathrm{R}$
– $\mathbf{P_{C1}P_1} \cdot \mathbf{P_{C0}P_{C1}} = 0$ and $\mathbf{P_{C0}P_0} \cdot \mathbf{P_{C0}P_{C1}} = 0$

This positioning method requires the numerical resolution of a system of four equations with four unknowns and guarantees tangency of the cutter with the directrix curves. At this stage, it is close to positioning Stute [5].

The positioning method known as improved positioning presented in [7–9] involves first setting the cutter in the standard positioning configuration and making a rotation about an axis calculated from the normals to the surface at the

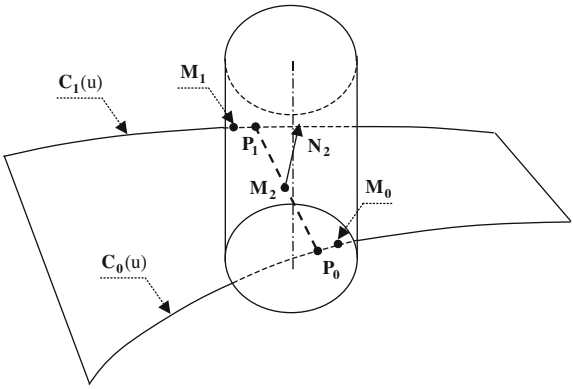

Fig. 2.16 Improved positioning

ends of the rule. This method is based on searching for two points of tangency between the cutter and the two directrices and a point of contact on the rule considered. This was first developed for a cylindrical cutting tool.

The conditions for bringing into position are as follows (Fig. 2.16):

- contact between the rule $[\mathbf{P_0P_1}]$ and the cutter at point $\mathbf{M_2}$,
- tangency with the two directrix curves $\mathbf{C_0}(u)$ and $\mathbf{C_1}(u)$ on either side of the end points of the rule: points $\mathbf{M_0}$ and $\mathbf{M_1}$.

Working from these imposed parameters and conditions, positioning involves resolution of a non-linear system of seven equations with seven unknowns. The cutter position is then defined by the angle γ between the axis of the cutter (with rotation going about the axis $\mathbf{N_2}$ defined on standard positioning) and the rule, and by the position of point $\mathbf{M_2}$ on the rule.

It transpires from this study that improved positioning generates a geometric error considerably less than that produced by other positioning strategies. This can be explained by the fact that the points characteristic of improved positioning $\mathbf{M_0}$, $\mathbf{M_1}$ and $\mathbf{M_2}$ are generator points. It was shown [9] that the points of tangency on the directrices are generator points. Thus, although ascertained purely geometrically, improved positioning has interesting kinematic properties.

Improved positioning as previously presented is based on the axis $\mathbf{y_2} = \mathbf{N_2}$ defined by standard positioning. The axis $\mathbf{y_2}$ was imposed without knowing the influence it could have on machining error. The following evolutions are thus proposed for positioning:

- 1st positioning: the axis of rotation $\mathbf{y_2}$ is made to coincide with the bissectrix of the normals $\mathbf{N_0}$ and $\mathbf{N_1}$, this is known as "improved positioning",
- 2nd positioning: the point of rotation $\mathbf{M_2}$ is made to coincide with the middle of the rule; this positioning is known as centred improved positioning and the axis of rotation $\mathbf{y_2}$ is unknown,
- 3rd positioning: the axis of rotation $\mathbf{y_2}$ is chosen such that undercut and overcut errors are equal.

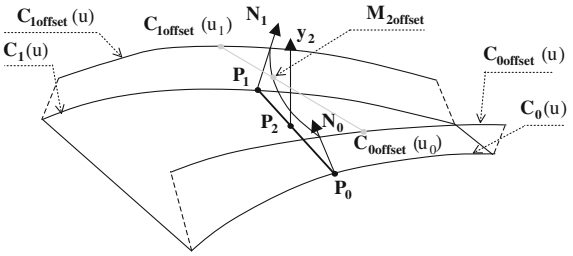

Fig. 2.17 Improved positioning applied to the offset surface

Among the different versions of improved positioning developed, centred improved positioning is the most efficient from the perspective of the error caused.

In [10, 11], an enhancement of improved positioning was proposed based on the offset surface of $\mathbf{S}(u, v)$. Improved positioning and its different versions were thus applied between the axis of the cutter and the offset surface $\mathbf{S_{offset}}(u, v) = \mathbf{S}(u, v) + R \cdot \mathbf{N}(u, v)$ (Fig. 2.17). The latter positioning method follows the same principle as the previous ones: a rotation of the cutter axis about the axis $\mathbf{y_2}$ is performed and the centre of rotation is located on $\mathbf{M_{2offset}} = \mathbf{M_2} + R \cdot \mathbf{N_2}$. A position of the axis going through $\mathbf{M_{2offset}}$ is sought that cuts through the two offset directrices $\mathbf{C_{0offset}}(u) = \mathbf{C_0}(u) + R \cdot \mathbf{N}(u, 0)$ and $\mathbf{C_{1offset}}(u) = \mathbf{C_1}(u) + R \cdot N(u, 1)$. Geometric positioning of the cutter axis can be expressed as follows:

- vector $\mathbf{M_{2offset}C_{0offset}}(u_0)$ is perpendicular to the axis of rotation $\mathbf{y_2}$,
- vector $\mathbf{M_{2offset}C_{1offset}}(u_1)$ is perpendicular to the axis of rotation $\mathbf{y_2}$,
- points $\mathbf{C_{0offset}}(u_0)$, $\mathbf{C_{1offset}}(u_1)$ and $\mathbf{M_{2offset}}$ are aligned as they all belong to the cutter axis

The positioning applied to the offset surface is of interest as it is easy to implement the system to be resolved consisting of three equations and three unknowns. When compared with improved positioning it shows undercut and overcut errors that are extremely close leading to giving preference to positioning on the offset surface if only error values are focused on. However, tangency on the directrices cannot be guaranteed as these conditions are no longer imposed and if tangency is sought, improved positioning offers the best option.

All the above reasoning was developed for cylindrical cutters, but improved positioning can also be used for conical cutters. Conical cutters are frequently used for turbine and fan blade-type workpieces as they involve problems of accessibility and cannot be machined with a cylindrical cutter of a reasonable diameter.

Improved positioning of the conical cutter proposed in [8], [12–14] (Fig. 2.18) is characterised by two points of tangency and one point of contact between the cutter and the surface, as for the cylindrical cutter. This positioning is obtained by a rotation of the cutter by an angle γ about an axis $\mathbf{N_2}$ at point $\mathbf{M_2}$ from the rule considered.

As the conical cutter has an evolving radius that has to be taken into account in the search for positioning, a new geometrical parameter g_0 called the guard is

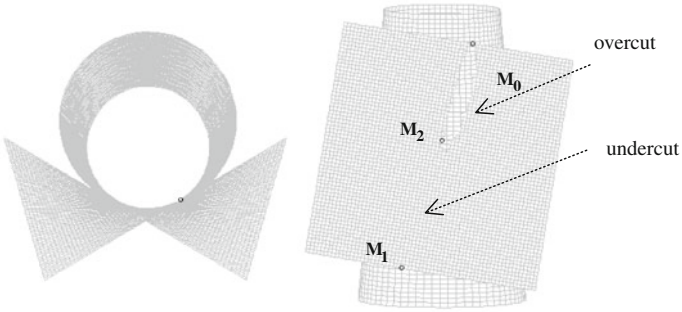

Fig. 2.18 Positioning the conical cutter

Fig. 2.19 Conical cutter parameters

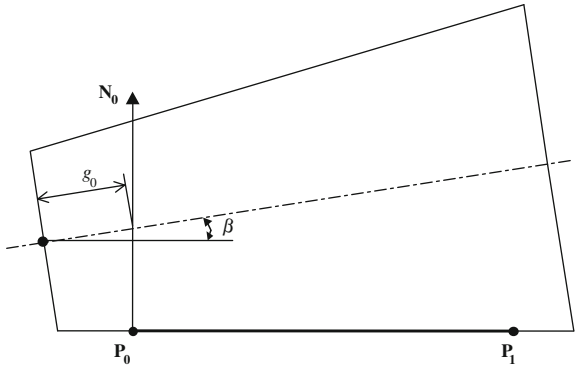

defined (Fig. 2.19). The guard is the distance, along the cutter axis, between the end point of the cutter and the osculating plane on $\mathbf{P_0}$. The guard is initially set by the user. Cutter positioning is thus fully defined by the three following parameters:

- the angle γ between the rule and the cutter axis projected in the plane having the vector $\mathbf{N_2}$ as normal,
- the position of point $\mathbf{M_2}$ on the rule,
- the guard g_0.

From these parameters and imposed conditions, positioning involves resolution of a non-linear system of seven equations with seven unknowns. This system is resolved numerically by the Newton–Raphson method. Quantitative analysis of error is also proposed by Monies [13], this being addressed in the paragraph "Assisting cutting tool choice".

The numerical positioning methods introduced impose geometric conditions (for distance and sometimes tangency) in order to establish a cutting tool's position. Many other positioning strategies were established using iterative methods

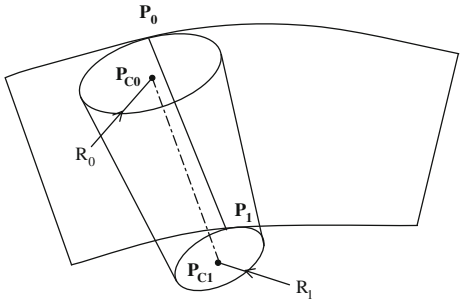

Fig. 2.20 Positioning Chiou

that involved modifying an initial positioning after error estimation and compensation. These iterative methods will now be presented in what follows.

The application of iterative methods requires knowledge of error so as to compensate for it. The geometrical error between the surface generated by a moving cutter and the nominal surface is determined using the following relation:

$$\mathbf{S}(u, v) + \varepsilon \mathbf{N}(u, v) = \mathbf{S}_{\mathbf{env}}(s, t) \tag{2.17}$$

$\mathbf{S}_{\mathbf{env}}(s, t)$ represents the envelope surface (or machined surface) corresponding to the trace left by the cutter. ε represents the distance between the machined surface and the nominal surface along the normal to the nominal surface.

In order to determine $\mathbf{S}_{\mathbf{env}}(s, t)$, the successive positions taken by the cutter need to be known so as to allow grazing curves dependent on the cutter speed vector to be established. A certain number of works cover the issue of envelope surfaces, noteworthy amongst which are [15, 16]. The grazing curve cannot be known without knowing the next position of the cutter, meaning that error computations based on a static position of the cutter can only be approximate.

Approximation methods of error calculation used for the development of new strategies were analysed and compared in [17]. The goal with these error calculation methods is to reduce computation times. Indeed, iterative methods that recalculate the envelope surface after each change in tool path are those that give greatest accuracy when calculating error but are detrimental to computation time. A number of error estimation methods have been devised to evaluate a strategy's accuracy rapidly. The various authors of these iterative methods seek a trade-off between positioning effectiveness and speed in obtaining the result. No attempt is made to rank the methods introduced below as they would all have to be implemented on the same computer to compare calculation times, with the error being calculated using Eq. 2.17.

The method developed in [18] is established for roughing and finishing of ruled surfaces. It can be applied to both cylindrical and conical cutters. The study is conducted iteratively and covers use of the cutter's envelope surface. Initially, a set of cutter positions is defined using relations 15 and 16 as already introduced (Fig. 2.20):

The envelope surface is calculated from the set of positions. For each cutter position, the author calculates the distance from the envelope curve to the ruled

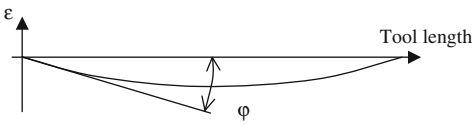

Fig. 2.21 Error profile

surface of the work-piece. The chosen positioning gives error profiles for overcut and maximum error, noted ε_{max}, is used to reposition the cutter:

$$\mathbf{P_{C0}} = \mathbf{P_0} + (\mathrm{R_0} + \varepsilon_{max})\,\mathbf{N_0} \tag{2.18}$$

$$\mathbf{P_{C1}} = \mathbf{P_1} + (\mathrm{R_1} + \varepsilon_{max})\,\mathbf{N_1} \tag{2.19}$$

The surface envelope and error are recomputed. The cutter will be repositioned until the overcut error becomes null. This procedure is used to rough cut the surface.

The finishing strategy is much in the same spirit. The cutter is first positioned using Eqs. 2.15 and 2.16. Having computed the envelope surface and the error profile between an envelope curve and the ruled surface, the cutter is offset for the error to be null on the directrices. The error profile obtained is shown in Fig. 2.21:

The cutter is then repositioned by a rotation of angle φ in the plane containing the cutter axis and the normal $\mathbf{N_0}$ at point $\mathbf{P_{C0}}$. As the envelope surface is modified, this repositioning procedure can be reiterated until there is no further overcut error. Finally, as this strategy leads to a significant undercut error, it is suggested that the surface be milled in several passes breaking down the ruled surface into several ruled surfaces. This study proposes an exact evaluation of error but has an adverse effect on computation time.

Lee and Suh [19] also propose an iterative positioning method where the cutter axis is initially taken to coincide with the considered rule and then translated along the direction $\mathbf{N}(\mathrm{u}, 0.5)$ by a distance d before a rotation of angle θ about the same axis is finally performed (Fig. 2.22).

For a set of couples (θ, d), cutter positioning is evaluated using a performance index $\mathrm{I_u} = \sum_{\mathbf{i}=1}^{\mathbf{n}} \left|\mathrm{d_{u,i}} - \mathrm{R}\right|$ with $\mathrm{d_{u,i}}$ the set of distances between n points of the cutter axis and the surface $\mathbf{S}(\mathrm{u}, \mathrm{v})$. The positioning retained will be that which gives the smallest value for the performance index $\mathrm{I_u}$.

For each value θ tested, the distance d minimising error is calculated. This calculation is based on an approximation of the surface $\mathbf{S}(\mathrm{u}, \mathrm{v})$using triangular patches.

In [20], a new form of iterative positioning is proposed (Fig. 2.23). The method works as follows:

- Initial positioning*:* the cutter is positioned using the method Bedi et al. [6] as introduced previously. The following hypothesis is then adopted: maximum error will be found at v = 0.5.
- First modification of initial positioning*:* The positioning established at this stage is identical to the previous one but uses points inside the rule rather than at the

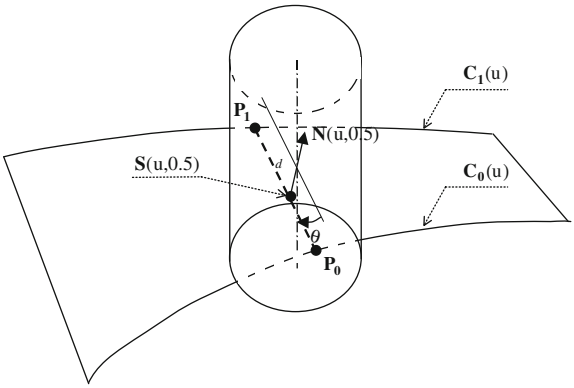

Fig. 2.22 Positioning Lee

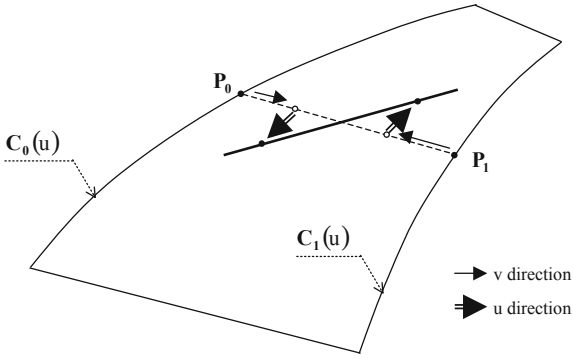

Fig. 2.23 Positioning Menzel

ends. To do so, the two positioning points of the cutter axis are translated in the direction of the rule (from the boundaries $v = 0$ and $v = 1$ up to the parametric value $v = 0.5$) by successive increments. On each iteration, the cutter position leads to a geometric error of the undercut type on the sides of the rule and overcut type in the middle. The error is close to that seen in Fig. 2.14 with Liu's positioning [4]. The position $[(u, v_1), (u, v_2)]$ retained is the one that minimises total error.

- Second modification of positioning*:* from solution $[(u, v_1), (u, v_2)]$, the positioning points of the cutter are translated along the isoparametrics $v = v_1$ and $v = v_2$. The positioning points of the cutter are characterised by: $[(u_1, v_1), (u_2, v_2)]$: parameters u_1 and u_2 are such that $(u - u_1)$ and $(u - u_2)$ have opposite signs. The positioning points of the cutter are translated until the minimum distance between the axis and the rule considered is equal to the cutter radius. A third point of tangency is then created on the rule. The rotation induced by this second optimisation is of the order of 5° at most.

[21] adapted a version of their positioning defined in [6] to conical cutters. The method proposed involves first bringing the cutter tangent to the two guide curves. These curves can be other than directrices of the ruled surface. The point where

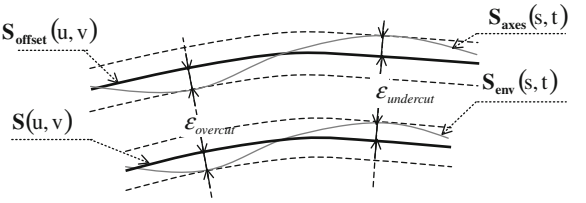

Fig. 2.24 Properties on offset surfaces

error reaches a maximum value is sought. The second stage allows maximum error to be reduced by moving the guide curves towards the point with the biggest deviation along the rule. This allows positioning error to be reduced by about a half. The third stage involves moving the cutter position along the feed direction to further reduce error between the given surface and the machined surface.

Finally, a last iterative positioning is presented in [22] under the method named "Three Points Offset" (T.P.O.). This method applies only to cylindrical cutters and involves positioning the cutter axis on the offset surface defined by:

$$\mathbf{S_{offset}}(u, v) = \mathbf{S}(u, v) + R\mathbf{n}(u, v) \tag{2.20}$$

The authors seek to minimise deviation between the offset surface and the axis as they show that maximum error between the offset surface $\mathbf{S_{offset}}(u, v)$ and the surface swept by the axis $\mathbf{S_{axis}}(s, t)$ is equal to the maximum error between the nominal surface $\mathbf{S}(u, v)$ and the envelope surface $\mathbf{S_{env}}(s, t)$ (Fig. 2.24).

"T.P.O." positioning involves positioning the cutter axis by three points belonging to $\mathbf{S_{offset}}(u, v)$. To do so, two points $\mathbf{P_{0offset}} = \mathbf{S_{offset}}(u, 0)$ and $\mathbf{P_{1offset}} = \mathbf{S_{offset}}(u, 1)$ belonging to the two directrices $\mathbf{C_{0offset}}(u)$ and $\mathbf{C_{1offset}}(u)$ of the offset surface (Fig. 2.25) will be considered. Point $\mathbf{P_{0offset}}$ is fixed throughout the argument and is located on the rule considered. Point $\mathbf{P_{1offset}}$ moves along the directrix $\mathbf{C_{1offset}}(u)$. For each position occupied by $\mathbf{P}_{1\mathbf{offset}}$, maximum error between the offset surface and segment $[\mathbf{P_{0offset}}\,\mathbf{P_{1offset}}]$ is calculated. The following assumption is made: maximum error is located on $v = 0.5$. The position of $\mathbf{P_{1offset}}$ minimising the value of that error will be kept to position the cutter.

The cutter axis is then defined by the two points $\mathbf{P_{0offset}} = \mathbf{S_{offset}}(u, 0)$ and $\mathbf{P_{1offset}} = \mathbf{S_{offset}}(u', 1)$. The error located at $v = 0.5$ is considered to be small enough to be able to state that $[\mathbf{P_{0offset}}\,\mathbf{P_{1offset}}]$ cuts the isoparametric curve $v = 0.5$.

The authors conclude by asserting that the cutter passes through the three isoparametric curves of the offset surface for values $v = 0$, $v = 0.5$ and $v = 1$. The cutter is then considered to be tangent at three points of the surface $\mathbf{S}(u, v)$.

A second stage is then implemented on all the axis positions calculated. By interpolation on the previously established axis positions, a B-spline surface is calculated. Then, from a cloud of points derived from the offset surface (Eq. 2.20), the B-spline surface is recalculated so as to minimise the quadratic sum of deviations between the cloud of offset points and the B-spline surface. This stage allows the ruled surface of the axis to be better distributed around the cloud of offset points.

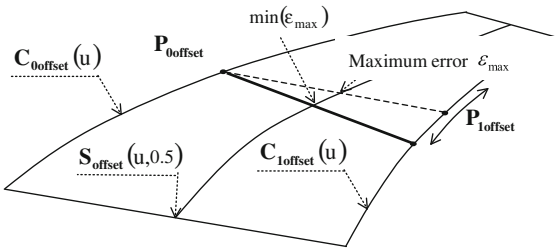

Fig. 2.25 "T.P.O." positioning for a cylindrical cutter

2.3 Free-Form Surfaces

The introductory paragraph to the present section described the gains that flank milling could contribute as compared with end milling. The idea developed in this paragraph is in devising methods for approximation of free-form surfaces into ruled surfaces with the aim of being able to flank mill those surfaces.

2.3.1 Discretising into Ruled Surfaces

Studying the geometry of ruled surfaces shows that the most influential parameter on interference is the twist α of the surface. In order to reduce interference, some authors recommend milling by strips [1, 18]. They break down the surface into several ruled surfaces. On each ruled surface, as the twist is smaller, the interference generated is thus reduced. However, none of the authors describe this breakdown and it is often taken in linear fashion on parameter v. Consider first for example in Fig. 2.26, a surface whose twist is constant and equal to 90° and where the ratio $\|\mathbf{T_0}\|/\|\mathbf{T_1}\|$ is constant and equal to 2 whatever the rule. Taking a linear breakdown of the ruled surface can prove to be relatively ineffective according to the ratio $\lambda = \|\mathbf{T_0}\|/\|\mathbf{T_1}\|$. It was decided to break down the surface into 2 ruled surfaces for v varying between $[0, 0.5], [0.5, 1]$. In Fig. 2.26, it can be seen that the twist of the first surface is equal to 27° while on the other it is 63° (90°−27°). This shows that a breakdown must be adapted to the surface in order to distribute the twist uniformly over the two surfaces. To do so, the breakdown must be made at $v = 0.67$. The twist for both surfaces will then be 45°. This breakdown can be constant if the ratio λ is constant over the entire surface. However, except for special cases, this remains untrue. When the ratio λ between the tangents is variable over the entire surface, for example between 1 and 2, and if a constant twist is desired on each surface, it will be necessary for any rule to adapt the value of v that cuts through the surfaces. This global positioning leads to having an axial engagement of the cutter that varies over the entire surface, which condition may be technologically undesirable.

Consider now (Fig. 2.26) having a surface with $\|\mathbf{T_0}\|/\|\mathbf{T_1}\|$ that varies from 1 to 2 and twist that is constant over the entire surface. Another solution involves

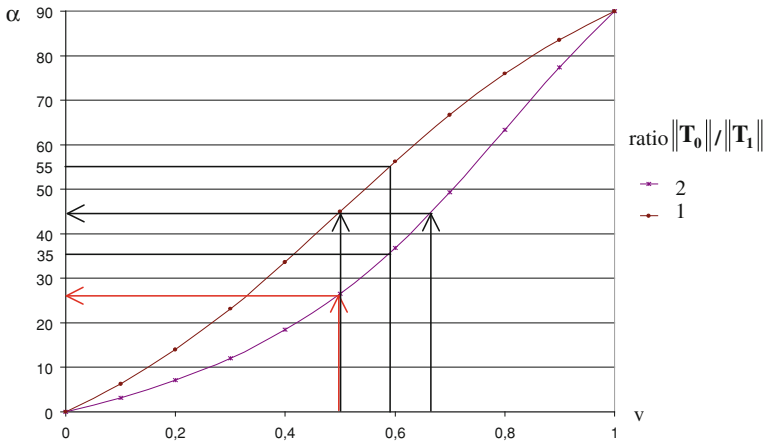

Fig. 2.26 Evolution of twist in relation to the ratio $\|\mathbf{T_0}\|/\|\mathbf{T_1}\|$

finding the value v that cuts the surface into two such that the maximum twist for each of the two surfaces is equal and minimal. In the example below, this value corresponds to $v = 0.58$. For the first surface, with v varying over the interval $[0; 0.58]$, the twist will evolve from 35° to 55° while for the second surface for v varying over the interval $[0.58; 1]$, the twist will go from 55° (90−35) to 35° (90−55). The distribution of twists will then be (35°; 55°) for both surfaces.

Breakdown into zones can provide an interesting alternative to reduce error. However, this breakdown has to be precise in order to reduce error and thus allow larger sized cutters to be chosen. The positioning methods employed must absolutely respect the directrices when strip milling, otherwise the entire surface machined is likely to show steps on the transition zones between strips.

With a view to extending ruled surface flank milling methods to free-form surfaces, Elber et al. [23, 24] propose an algorithm for discretising free-form surfaces into ruled surfaces. The authors apply their algorithm on a B-spline surface:

$$\mathbf{S}(u, v) = \sum_{i=0}^{n} \sum_{j=0}^{t} \mathbf{P_{ij}}\, N_{i,m}(u) N_{j,r}(v) \tag{2.21}$$

where the points $\mathbf{P_{ij}}$ constitute the characteristic network of the patch.

The surface with any shape $\mathbf{S}(u, v)$ will be discretised into a number of ruled surfaces $\mathbf{R_k}(u, v)$. Let $\mathbf{R_k^*}(u, v)$ be the representation of $\mathbf{R_k}(u, v)$ in the same B-spline base as that for $\mathbf{S}(u, v)$. After this surface manipulation, the following is obtained:

$$\mathbf{R}^*(u, v) = \sum_{i=0}^{n} \sum_{j=0}^{t} \mathbf{Q_{ij}^*}\, N_{i,m}(u)\, N_{j,R}(v) \tag{2.22}$$

The following inequality provides the limit distance corresponding to the approximation granted between $\mathbf{S}(u, v)$ and the ruled surface $\mathbf{R_k^*}(u, v)$.

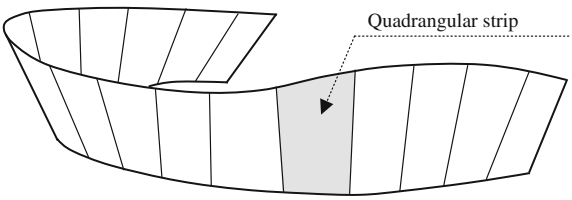

Fig. 2.27 Approximation of the surface by quadrangular strips

$$\left\| \mathbf{S}(u,v) - \mathbf{R}_{\mathbf{k}}^{*}(u,v) \right\| \leq \mathrm{Max} \left\| \mathbf{P}_{\mathbf{ij}} - \mathbf{Q}_{\mathbf{ij}}^{*} \right\| \tag{2.23}$$

If this distance exceeds the accuracy of discretising, the surface $\mathbf{S}(u,v)$ will be discretised in two surfaces to which the previous procedure will be applied. Adopting this methodology, a free-form surface can thus be discretised into ruled surfaces, with a given accuracy. Obviously, it is important after this approximation phase to conduct a study of the visibilities permitting detection of the surfaces that can actually be flank milled.

Other methods exist based on the idea of approximating the surface by developable ruled surfaces rather than seeking to position the cutter locally on the surface to minimise error. Software positioning can be used to machine the developable ruled surface free of interference. The machining error induced is thus managed during the approximation phase for the surface rather than in terms of cutter positioning: the machining error is then the approximation error.

In [25], the authors propose to approximate the surface using developable ruled surfaces of the Bezier patch type connected in tangency. Tsai et al. [26] propose an approximation of the surface $\mathbf{S}(u,v)$ using developable ruled surfaces of the quadrangular type (Fig. 2.27). The authors propose an algorithm for automatic generation of quadrangular strips minimising approximation error.

The algorithm developed is based on the existing Dijkstra algorithm (algorithm minimising the areas of quadrangles) and is adapted to the problematic flank milling to take approximation to its conclusion with the aim of minimising geometrical error.

The construction of quadrangular strips answers to the following constraints (Fig. 2.28):

- the length of the cutter must be greater than the set of distances $[\mathbf{P_{0,j}}, \mathbf{P_{1,j}}]$ (note $\mathbf{P_{i,j}}$ the **j**th quadrangle crest located on the directrix $\mathbf{C_i}(u)$),
- the relative speed between two consecutive crests $\left\| v_{\mathbf{i,j}} - v_{\mathbf{i,j+1}} \right\|$ must not vary excessively, the aim being to limit cutter acceleration and deceleration phenomena:
- $v_{\mathbf{i,j}} = \dfrac{\mathbf{P_{i,j}} - \mathbf{P_{i,j-1}}}{t}$ (t being the time the cutter takes to go between points $\mathbf{P_{i,j-1}}$ and $\mathbf{P_{i,j}}$),
- changes in the direction of speed between two consecutive crests $\dfrac{v_{\mathbf{i,j}} \cdot v_{\mathbf{i,j+1}}}{\left\| v_{\mathbf{i,j}} \right\| \left\| v_{\mathbf{i,j+1}} \right\|}$ are limited,
- the twist on each quadrilateral is limited: $\theta_{\mathbf{j}} = a\cos\left(\dfrac{(\mathbf{P_{1,j}} - \mathbf{P_{0,j}}) \cdot (\mathbf{P_{1,j+1}} - \mathbf{P_{0,j+1}})}{\left\| \mathbf{P_{1,j}} - \mathbf{P_{0,j}} \right\| \left\| \mathbf{P_{1,j+1}} - \mathbf{P_{0,j+1}} \right\|} \right)$

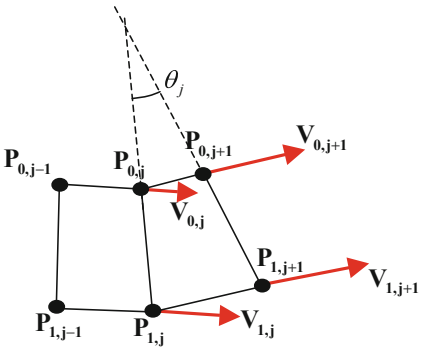

Fig. 2.28 Constraints applied to quadrangular surfaces

2.3.2 Local Positioning

Some authors have taken an interest in flank milling of free-form surfaces without going through discretising into ruled surfaces, whether developable or not. As these works are based on the differential geometry of the surfaces, they have to be of continuity C^2 to be able to approximate to the second order, locally at the points of contact, the surfaces of the cutter and the workpiece.

Angular positions for the cutter excluding interference can be determined working from the local topology of surfaces defined by the sign of the main curvatures of the workpiece. These angular positions are those of the principal directions [27, 28] of the cutter in relation to those of the surface.

According to the machining tolerance, the width milled can be calculated through working out the distances between the surfaces of the cutter and the workpiece approximated by their curvatures.

Along similar lines, works [29] address calculation of the Dupin indicatrices for the cutter surface, the cutter envelope surface and the surface of the workpiece in order to determine possible interference. The method applies both to end milling and flank milling. The same authors [30] develop the results of previous works to propose a local optimisation of positioning to maximise the width machined while minimising the normal relative curvature between the envelope surface of the cutter and the surface of the workpiece.

These methods will not be further developed in this chapter as their applications remain limited to relatively tight surfaces (important curvature radius) and the risks of local and global collision remain high. Their application requires a collision management tool.

2.3.3 Global Cutter Positioning Methods

All the methods presented allow a tool path comprising two sets of points characterising the positions taken successively by the cutter axis for each rule

considered to be defined. Some authors devote attention to the totality of distances between the envelope surface and the nominal surface with a view to optimisation established from a variety of criteria. These works follow from studies conducted into local positioning. The results obtained after resolution of major systems of equations need to be considered circumspectly from a numerical point of view.

Two main objectives justify the formulation of an optimisation problem:

- minimisation of geometric error when the positioning used does not allow the values set by shape tolerance on the surface to be achieved,
- fluidity of the tool path so as to anticipate machining defects due to excessively abrupt cutter movements, especially when using cutter positioning in high speed machining.

In [31–33], the argument developed is based on a compensation of theoretical error. The idea is to position the cutter simply and in a non-optimised fashion while remaining aware that such positioning will be the source of error. Optimisation of positioning is a trade-off between the error induced by cutter placement and the fluidity of the path obtained.

The method proposed can be broken down as follows:

- calculation of the set of cutter positions enabling the surface to be milled. The positioning method is not defined, the only constraint being its simple implementation. The two sets of points characterising positioning of the cutter axis are interpolated into 2 B-spline curves.
- applying a grid on the surface to be machined $\mathbf{S}(u, v)$. At each point of this grid, the distance corresponding to the error between the surface to be machined and the envelope surface generated by the cutter is calculated thus obtaining a grid of positioning errors over the entire surface.
- displacement of the poles of the envelope surface of the cutter in order to minimise the quadratic sum of errors using the small displacement method. By modifying the envelope surface, all cutter positionings are modified.
- a last stage is implemented integrating into the optimisation problem a fluidity criterion based on the deformation energy of each of the guide curves of the axis-cutter surface. This stage was added to find a trade-off between machining precision and fluidity of the path.

In [34], the authors rely on local positioning using the method developed by Liu [4]. They then interpolate this discrete set of positions to generate a NURBS surface. This surface is generated as the envelope of the previously defined cylinders. They then seek to minimise the error between the ruled surface and the envelope surface. To do so, the check points of the NURBS are adjusted. The Downhill Simplex method in Multidimensions is used to optimise its translation and rotation components for each check point so as to minimise error in relation to the ruled surface. No additional information is provided as to how optimisation is obtained.

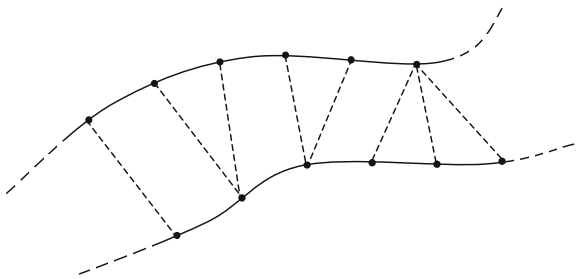

Fig. 2.29 Construction of lines of contact

The works presented in [35] focus on global optimisation of positioning from a cloud of points. Initially, a certain number of position settings are calculated on different rules using the method developed by Chiou [18]. This approach has the advantage of being easy to implement. Two sets of points corresponding to the cutter axis are obtained. Each set of points is then interpolated by a cubic B-spline curve in order to obtain an equation of the ruled surface swept by the cutter axis. This equation is then used to calculate the cutter's envelope surface.

Using a cloud of points on the surface of the workpiece, the distance from these points to the envelope surface of the cutter is computed. The authors then pose an optimisation problem that seeks to minimise the maximum distance between the envelope surface of the cutter and the surface of the workpiece taking the cloud of points as a base. Using an approximation to the first order of the distance function, the problem is then linearised and its resolution leads to obtaining new centre–cutter points. To obtain a first positioning that is more effective than that proposed by Chiou [18], they suggest performing a minimisation of the quadratic distance of the points of the workpiece to the envelope surface. The optimisation method leads to a reduction in maximum error but implementation often remains a delicate matter and is costly in computation time without being assured of control over the final result in terms of path fluidity.

In [36], another global positioning approach is proposed. This method is based on approximating the directrices of the surface. The logic can be broken down into stages as follows (Fig. 2.29):

- discretising of the directrices $\mathbf{C_0}(u)$ and $\mathbf{C_1}(u)$ of the surface is performed.
- on one of the two directrices, for each point discretised, contact lines are created between the point concerned and the points of the opposite curve. Two criteria are to be respected in this stage: there must be no intersection between adjacent contact lines and there must be no "point jumping" on the opposite curve.
- each contact line is used as a cutter positioning support. The points for passes of the cutter axis $\mathbf{P_{C0}}$ and $\mathbf{P_{C1}}$ are calculated from the end points of the rule (Eq. 2.15 and 2.16).
- a program is used to define the optimum route (series of contact lines) to minimise error. The physical magnitude to be minimised is the machining error (this is estimated using the Z-buffer method), while the optimisation parameters are four in number:

- the choice of the number of points to be discretised on each directrix may be different between $\mathbf{C_0}(u)$ and $\mathbf{C_1}(u)$,
- the maximum number of contact lines that can be established for each point,
- the number of points the optimisation program chooses to jump between two adjacent lines of contact.
- the last parameter provides an opportunity to discretise between the two directrix curves of the surface. It gives the number of isoparametric curves on v that will be used as a support for approximation. This is equivalent to strip milling.

This original method is difficult to compare with the other global methods whether from the perspective of results in terms of error or tool path fluidity.

2.4 Assisting Cutting Tool Choice

All the studies presented using analytical or numerical methods, whether iterative or not, aim to reduce error between the nominal surface and the envelope surface corresponding to the machined surface. The final objective is not to cancel out the error but to be able to use the largest cutting tool while also respecting machining tolerance. Indeed, theoretically it is possible to cancel error if the cutter radius is null. In this case, the cutter will be a line applied to coincide with the rule. If accessibility were possible, wire electrical discharge machining would be the process best suited to obtain the surface sought exactly. From a technological point of view, to limit cutter vibration and bending [37, 38], it is necessary to have the biggest cutter (assuming there is no risk of collision with other surfaces). Now, in all the studies presented, the cutter shape and dimensions are chosen right from the start. If finally, positioning were to lead to an error greater than the tolerance, the entire strategy would have to be thought out again and recalculated using a cutter with other dimensions. With the aim of avoiding this repetition, it seemed advantageous to predict the error with the goal of defining a cutter with dimensions to match the machining tolerance. The influence of the radius R was shown in [13]: it modifies errors in amplitude but does not change the general shape of the error curves. The problem posed thus relates to being able to choose a cutter radius that will lead to an error lower than the tolerance interval imposed by the surface.

The idea of helping to choose the cutter radius does not involve adopting an iterative logic where the algorithm is repeated until the value of the radius giving maximum permitted error is found. On the contrary, the goal is to run the algorithm just once, choosing a cutter radius arbitrarily and then being able, without further calculation, to give the maximum radius to be chosen for the cutter. To achieve this objective, the relation between the cutter radius and the error caused has to be highlighted. Furthermore, it was noted that the zones on the surface where maximum error occurred were those where twist was maximal.

To choose the cutter maximum radius, the position of the cutter on the rule where twist is maximal will need to be calculated.

Some of the authors behind the positioning methods previously introduced propose assistance in choosing the cutter dimensions. Each method presented relates to the positioning developed.

The first analytical positioning mentioned is that implemented in many CAD/CAM software packages. An algebraic calculation of the maximum cutter diameter allowing for the tolerance interval to be respected remains possible:

$$\mathrm{R} = \frac{\varepsilon_{\max}(\varepsilon_{\max} - 2\rho_{\mathbf{1}})}{2[\rho_{\mathbf{1}}(\cos\alpha - 1) + \varepsilon_{\max}]} \tag{2.24}$$

Rubio [3] proposes a numerical calculation of the maximum cutter diameter. The radius is obtained by resolution of the system with three equations and three unknowns $(\mathrm{R}, \alpha_{\mathbf{0}}, \alpha_{\mathbf{1}})$ as shown below:

$$\begin{cases} \rho_{\mathbf{0}} + \mathrm{R} - \sqrt{\mathrm{R}^{\mathbf{2}} + \rho_0^2 + 2\,\rho_0\,\mathrm{R}\,\cos\alpha_0} = \varepsilon_{\max} \\ \rho_{\mathbf{1}} + R - \sqrt{\mathrm{R}^{\mathbf{2}} + \rho_{\mathbf{1}}^2 + 2\,\rho_{\mathbf{1}}\,\mathrm{R}\,\cos\alpha_{\mathbf{1}}} = \varepsilon_{\max} \\ \alpha = \alpha_{\mathbf{0}} + \alpha_1 \end{cases} \tag{2.25}$$

Liu [4] also proposes a method for numerical resolution to calculate the cutter diameter, but this is an iterative method based on Eqs. 2.11, 2.12 and 2.13.

The work by [10] highlighted the quasi-linear relation existing between the cutter radius and the error caused: $\frac{\varepsilon}{\mathrm{R}} \approx$ constant. A study was conducted to show that the linear model was the most effective and that, contrary to what one might have assumed, developing a higher degree model would lead to less accurate results. The effectiveness of the linearity hypothesis can be explained by studying the radius of curvature of the function $\varepsilon(\mathrm{R})$; as the latter is extremely significant; the hypothesis of linearity between the geometric error and the cutter radius is justified. Working from a first cutter radius R_0 and the maximum error value ε_0 obtained after positioning, the optimum cutter radius can be calculated by linearising the function $\varepsilon(\mathrm{R})$. The optimum radius is obtained by:

$$\mathrm{R}_{\max} = \frac{\varepsilon_{\max}}{\varepsilon_0}\mathrm{R}_0 \tag{2.26}$$

$\varepsilon_{\max}$ is the maximum error permissible by the profile tolerance of the surface.

Looking at the error curves published for the various local positioning strategies in the previous works, different curve shapes were identified. Some curves are of the overcut/overcut type, while others are of the undercut/overcut or even overcut/undercut types. The idea developed in this paragraph is to seek to better understand and forecast the type of curve positioning will lead to. The forecasting method described below was developed in relation to improved positioning [10, 39]. It can also be applied to other methods.

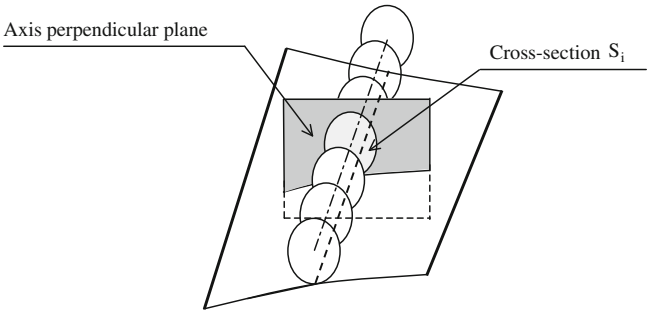

Fig. 2.30 Cutter discretising

The reasoning here can be summarised as follows:

- the cutter is discretised by parallel planes perpendicular to the axis. Cross-sections S_i (Fig. 2.30) are obtained,
- for each positioning, the real displacement Δ_{ri} imposed on the cross-section S_i by the adopted strategy is calculated,
- for each cross-section S_i, the displacement Δ_{ti} that would be necessary to ensure tangency with the surface is calculated,
- a conclusion is reached as to the nature of the error induced in each cross-section by comparing Δ_{ri} with Δ_{ti}.

In order to understand how error forecast functions are implemented, it will first be useful to remind of improved positioning in detail:

- Stage 1: the axis of the cutter is parallel to the rule considered
- Stage 2: the cutter is translated along a direction $\mathbf{y_2}$ by the value of its radius R. Two overcut errors can then be seen on either side of point $\mathbf{M_2}$ where the normal to the surface coincides with $\mathbf{y_2}$.
- Stage 3: the cutter is turned about the axis $(\mathbf{M_2}, \mathbf{y_2})$ by a value γ. The amplitude γ of this rotation is calculated to ensure tangency with $\mathbf{C_0}(u)$ and $\mathbf{C_1}(u)$. When rotation takes place, the circular cross-section becomes an ellipse, and with angle γ remaining low, it can be assumed that the cross-section remains circular.

Considering the cross-sections independently of each other, the problem can be modelled simply (Fig. 2.31). The intersection between the surface and the plane containing the cutter cross-section is a curve whose radius of curvature can be considered to be locally constant.

The displacement Δ_{ti} needed to ensure tangency between the cutter and the surface on the cross-section considered is calculated geometrically:

$$\Delta_{ti} = \sqrt{(R + \rho_i)^2 - (R + \rho_i \cos(\alpha_i))^2} - \rho_i \sin(\alpha_i) \tag{2.27}$$

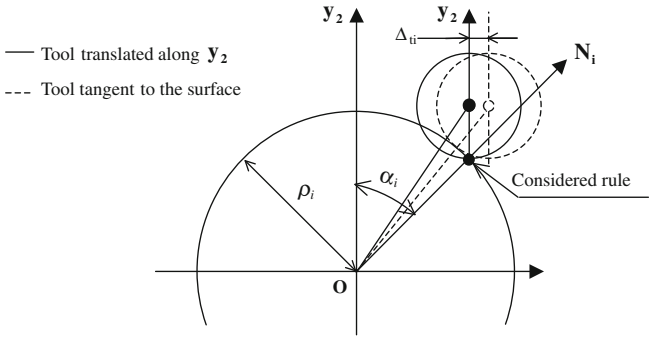

Fig. 2.31 Modelling the displacement of each cross-section

As the cutter is considered to be non-deformable, the real displacement Δ_{ri} for each cross-section is calculated by a linear interpolation between the two end cross-sections of the cutter Δ_0 and Δ_1 that are tangent to the surface:

$$\Delta_{ri} = (1 - v)\Delta_0 + v\Delta_1 \tag{2.28}$$

with

$$\Delta_0 = \sqrt{(R + \rho_0)^2 - (R + \rho_0 \cos(\alpha_0))^2} - \rho_0 \sin(\alpha_0) \tag{2.29}$$

$$\Delta_1 = -\left[\sqrt{(R + \rho_1)^2 - (R + \rho_1 \cos(\alpha_1))^2} - \rho_1 \sin(\alpha_1)\right] \tag{2.30}$$

with $\alpha_0 > 0$ and $\alpha_1 > 0$.

To conclude on the type of error obtained on the cross-section, it is sufficient to compare the displacement Δ_{ti} allowing tangency to be ensured with the real displacement of cross-section Δ_{ri} (Fig. 2.32).

- if $|\Delta_{ri}| < |\Delta_{ti}|$ and of the same sign, displacement of the cross-section will not be sufficient to ensure tangency and there is overcut,
- if $|\Delta_{ri}| > |\Delta_{ti}|$ and of the same sign, displacement of the cross-section is greater than that needed to ensure tangency and there is undercut,
- if $|\Delta_{ri}| = |\Delta_{ti}|$ there is tangency between the cutter and the surface on that cross-section,
- if $\Delta_{ri} \cdot \Delta_{ti} < 0$ the type of error is difficult to analyse as it depends on the orientation of angle α_i.

Geometric error can be estimated (Fig. 2.33) by the relation [39]:

$$\varepsilon_i = (\Delta_{ti} - \Delta_{ri}) \sin(|\alpha_i|) \tag{2.31}$$

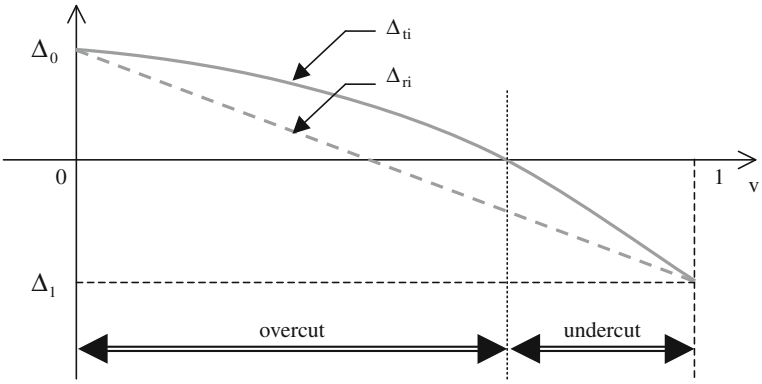

Fig. 2.32 Analysis of the type of error

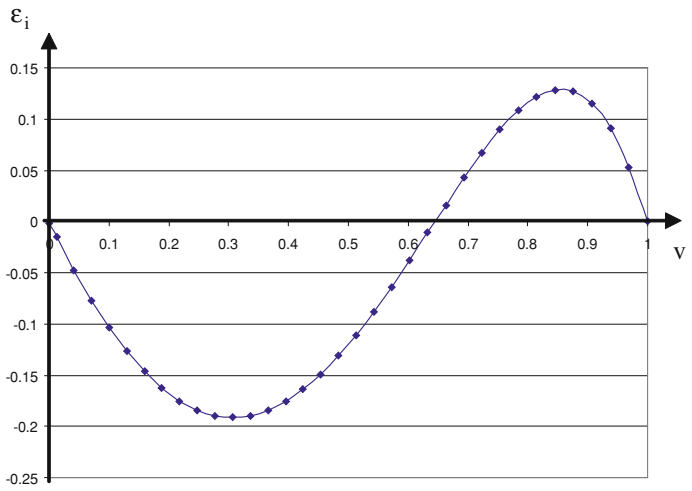

Fig. 2.33 Error estimation

The error corresponds to the difference in displacement $(\Delta_{ti} - \Delta_{ri})$ projected onto the normal to the surface at the point considered. This method of forecasting is especially advantageous as it allows errors to be evaluated instantaneously and another cutter to be chosen without having to calculate positioning. It can be readily applied to other types of local positionings and to other cutter geometries (conical cutters for example) and allows error to be estimated.

While linearity between the error and the radius of a cylindrical cutter allows the appropriate cutter to be determined, the same does not apply for the conical cutter. The choice of cutter dimensions for the conical cutter is given below.

Two independent parameters define the cross-section of the conical cutter: R_m and β.

- R_m: the minimum radius (at the end of the conical part)
- β: the half angle at the crest of the conical cutter

Initial entering of a radius R_{m_0} and a half angle at the crest β_0 taken technologically as large as possible, the algorithm developed by [13] allows optimal couples of cutters (R_{m_i}, β_i) to be obtained with a minimum number of iterations, such that the error obtained ε verifies:

$$\varepsilon \leq \varepsilon_{max} \tag{2.32}$$

This determination is made for a given position of rule and guard characteristic of maximum errors (significant twist). If the cutter sought keeps a half angle at the crest constant and equal to β_0 the relation of linearity (Eq. 2.26) can be retained, otherwise a procedure by dichotomy has to be implemented to determine the couples $(R_m, ,\beta)$ that respect the tolerance. In this manner a series of solution couples is obtained enabling the operator to select the appropriate cutter from the store.

References

1. Chaves-Jacob J (2009) Développement d'une méthodologie de réduction des défauts géométriques : application à l'usinage five-axis de composants de turbomachine. Thèse de doctorat. Arts et Métiers ParisTech, Cluny
2. Chavez-Jacob J, Poulachon G, Duc E (2009) New approach to 5-axis flank milling of free-form surfaces: computation of adaptated tool shape. Comput Aided Des 41:918–929
3. Rubio W (1993) Génération de trajectoires du centre de l'outil pour l'usinage de surfaces complexes sur machines à trois et cinq axes. Thèse de doctorat, Université Paul Sabatier Toulouse, France
4. Liu XW (1995) Five axis NC cylindrical milling of sculptured surfaces. Comput Aided Des 27:887–894
5. Stute G, Storr A, Sielaff W (1979) NC programming of ruled surfaces for five axis machining. Annals of the CIRP 28:267–271
6. Bedi S, Mann S, Menzel C (2003) Flank milling with flat end milling cutter. Comput Aided Des 35:293–300
7. Redonnet JM, Rubio W, Dessein G (1998) Side milling of ruled surfaces-Optimum positioning of the milling cutter and calculation of interference. Int J Adv Manuf Technol 14:459–465
8. Monies F, Rubio W, Redonnet JM, Lagarrigue P (2001) Comparative study of interference caused by standard and improved positioning of a conical milling cutter working on a ruled surface. J Eng Manuf (Part B) 215:1305–1317
9. Senatore J, Monies F, Redonnet JM, Rubio W (2005) Analysis of improved positioning in five-axis ruled surface milling using envelope surface. Comput Aided Des 37:989–998
10. Senatore J (2007) Analyse qualitative des parametres influents pour la planification des trajectoires sur surfaces gauches. Thèse de doctorat, Université Paul Sabatier Toulouse, France
11. Senatore J, Monies F, Landon Y, Rubio W (2008) Optimising positioning of the axis of a milling cutter on an offset surface by geometric error minimisation. Int J Adv Manuf Technol 37:861–871

12. Monies F, Redonnet JM, Rubio W, Lagarrigue P (2000) Improved positioning of a conical mill for machining ruled surfaces: application to turbine blade. J Eng Manuf (Part B) 214:625–634
13. Monies F (2001) Positionnement hors interférence pour l'usinage en bout et en roulant des surfaces gauches. Thèse de doctorat, Université Paul Sabatier Toulouse, France
14. Monies F, Felices JN, Rubio W, Redonnet JM, Lagarrigue P (2002) Five-axis NC milling of ruled surfaces: optimal geometry of a conical tool. Int J Prod Res 40:2901–2922
15. Peternell M, Pottmann H, Steiner T, Zhao H (2005) Swept volumes. Comput Aided Des Appl 2:599–608
16. Abdel-malek K, Yeh HJ (1997) Geometric representation of the swept volume using Jacobian rank-deficiency conditions. Comput Aided Des 29:457–468
17. Li C, Bedi S, Mann S (2005) Error measurements for flank milling. Comput Aided Des 37:1459–1468
18. Chiou JCJ (2004) Accurate tool position for five-axis ruled surface machining by swept envelope approach. Comput Aided Des 36:967–974
19. Lee JJ, Suh SH (1998) Interference-free tool-path planning for flank milling of twisted ruled surfaces. Int J Adv Manuf Technol 14:795–805
20. Menzel C, Bedi S, Mann S (2004) Triple tangent flank milling of ruled surfaces. Comput Aided Des 36:289–296
21. Li C, Bedi S, Mann S (2006) Flank milling of a ruled surface with conical tools–an optimization approach. Int J Adv Manuf Technol 29:1115–1124
22. Gong H, Cao LX, Liu J (2005) Improved positioning of cylindrical cutter for flank milling ruled surface. Comput Aided Des 37:1205–1213
23. Elber G (1995) Model fabrication using surface layout projection. Comput Aided Des 27:283–291
24. Elber G, Russ F (1997) 5-axis freeform surface milling using piecewise ruled surface approximation. ASME J Eng Ind 119:383–387
25. Chu CH, Chen JT (2006) Tool path planning for five-axis flank milling with developable surface approximation. Int J Adv Manuf Technol 29:707–713
26. Tsai WL, Wang CCL, Chu CH, Tang K (2008) Optimal quadrangulation of a strip for flank milling. Comput Aided Des Appl 5:307–315
27. Marciniak K (1987) Influence of surface shape on admissible tool positions in five-axis face milling. Comput Aided Des 19:233–236
28. Marciniak K (1991) Geometric Modelling for Numerically Controlled Machining. Oxford Science Publications, New York
29. Gong H, Cao L, Liu J (2008) Second order approximation of tool envelope surface for 5-axis machining with single point contact. Comput Aided Des 40:604–615
30. Gong H, Fang FZ, Hu XT, Cao L, Liu J (2010) Optimization of tool positions locally based on the BCELTP for 5-axis machining of free-form surfaces. Comput Aided Des 42:558–570
31. Lartigue C, Duc E, Affouard A (2003) Tool path deformation in 5-axis flank milling using envelope surface. Comput Aided Des 35:375–382
32. Pechard PY (2009) Génération de trajectoires d'usinage grande vitesse 5 axes par flanc d'outil: intégration d'un critère de fluidité. Thèse de doctorat, Ecole Normale Supérieure de Cachan, France
33. Pechard PY, Tournier C, Lartigue C, Lugarini JP (2009) Geometrical deviations versus smoothness in 5-axis high-speed flank milling. Int J Mach Tools Manuf 49:454–461
34. Xia J, Ge QJ (2000) Kinematic approximation of ruled surfaces using nurbs motions of a cylindrical cutter. Proceeding of DETC'00, ASME 2000 Design Engineering Technical Conferences. Baltimore, Maryland
35. Zhang XM, Zhu LM, Zheng G, Ding H (2010) Tool path optimisation for flank milling ruled surface based on the distance function. Int J Prod Res 48:4233–4251
36. Wu PH, Li YW, Chu CH (2008) Optimized tool path generation based on dynamic programming for five-axis flank milling of ruled surface. Int J Mach Tools Manuf 48:1224–1233

37. Larue A, Anselmetti B (2003) Deviation of a machined surface in flank milling. Int J Mach Tools Manuf 14:795–805
38. Landon Y, Segonds S, Lascoumes P, Lagarrigue P (2004) Tool Positioning Error (TPE) characterisation in milling. Int J Mach Tools Manuf 44:457–464
39. Senatore J, Landon Y, Rubio W (2008) Analytical estimation of error in flank milling of ruled surfaces. Comput Aided Des 40:595–603

http://www.springer.com/978-1-4471-2355-2

Machining of Complex Sculptured Surfaces
Davim, J.P. (Ed.)
2012, X, 258 p., Hardcover
ISBN: 978-1-4471-2355-2